Journal of ELECTRONIC MATERIALS, Vol. 45, No. 7, 2016
DOI: 10.1007/s11664-016-4487-4

Thermoelectric Properties of *n*-Type $Si_{0,8}Ge_{0,2}$-$FeSi_2$ Multiphase Nanostructures

ANDREY USENKO,[1,3] DMITRY MOSKOVSKIKH,[1,4] ANDREY KOROTITSKIY,[1,5] MIKHAIL GORSHENKOV,[1,6] ANDREY VORONIN,[1,7] DMITRY ARKHIPOV,[1,8] MARIA LYANGE,[1,9] GRIGORY ISACHENKO,[2,10] and VLADIMIR KHOVAYLO,[1,2,11]

1.—National University of Science and Technology "MISiS", Moscow 119049, Russia. 2.—ITMO University, St. Petersburg 197101, Russia. 3.—e-mail: usenko@misis.ru. 4.—e-mail: mos@misis.ru. 5.—e-mail: korotitskiy@misis.ru. 6.—e-mail: gorshenkov@misis.ru. 7.—e-mail: voronin@misis.ru. 8.—e-mail: hipa3@rambler.ru. 9.—e-mail: maria.lyange@gmail.com. 10.—e-mail: isachenko@inbox.ru. 11.—e-mail: khovaylo@misis.ru

We report on thermoelectric properties of *n*-type nanostructured bulk $Si_{0.8}Ge_{0.2}$ with the addition of $FeSi_2$ prepared via two sintering routes: the conventional spark plasma sintering method and a direct current pressing technique. The thermal conductivity, the electrical conductivity, and the Seebeck coefficient have been determined over the temperature range from 25°C to 900°C in a helium atmosphere. The highest ZT value for the multiphase nanostructured composite was reached at ~0.6 at 900°C. Embedding of 10 at.% $FeSi_2$ phase had a positive impact on thermal properties but dramatically affected the power factor, which eventually resulted in a drop of the thermoelectric efficiency. It was also shown that the orthorhombic β-FeSi2 phase transforms to a tetragonal α-FeSi2 phase during high temperature sintering.

Key words: Thermoelectric materials, spark plasma sintering, mechanical alloying, silicon germanium, iron disilicide, nanocomposite

INTRODUCTION

It is well known that waste heat is one of the main sources for energy loss. Thermoelectrics can be used for an efficient conversion of this waste heat. Among silicon compounds, silicon germanium (SiGe) has been the most promising thermoelectric for high temperature applications around 800°C. High mechanical strength and resistance to atmospheric oxidation make this material suitable for a number of practical applications.[1] For example, SiGe has been used in power generation systems of spacecraft for more than fifty years. The large-scale application of SiGe is limited for many reasons. The most important of them is the high price and a rather low thermoelectric efficiency. The thermoelectric efficiency of any material is determined by its dimensionless parameter figure of merit, $ZT = \frac{S^2\sigma T}{k}$, where S is the Seebeck coefficient, σ is the electrical conductivity, and k is the thermal conductivity.[1,2] The recent progress in increasing ZT has been mainly driven by a reduction of thermal conductivity via a nanostructuring approach.[3–7] It is well known that phonon and charge carrier transport are influenced by crystallite boundary scattering especially when the size of the crystallites is comparable to their characteristic lengths. If the crystallite sizes in the nanostructured material are comparable with the phonon mean free path but are larger than the charge carrier mean free path, the thermal conductivity is reduced more significantly than the electrical conductivity and this finally results in enhancement of ZT value. The efficiency of this approach has been demonstrated for a large group of the well known materials (Bi_2Te_3, SiGe, PbTe, Mg_2Si, etc.).[3,5–7] Another way to increase ZT value is to enhance electrical conductivity and the Seebeck coefficient or, in other words, the power factor of a thermoelectric material. This route can be

(Received June 17, 2015; accepted March 22, 2016; published online April 15, 2016)

realized by making a multiphase nanostructured composite.[8,9] It has been predicted theoretically[10] that embedding silicides into the host SiGe matrix can considerably improve thermoelectric properties of the multiphase material. The perspective of nanoparticle doping has also been introduced by a model calculation for silicides-SiGe alloy systems.[10] Several silicide-SiGe composite systems have been considered as perspective systems for the enhancement of ZT. However, experimental investigation of these material systems has been performed only for several SiGe-silicides composites with the addition of $CrSi_2$, $MoSi_2$, and WSi_2.[11–14] Virtually the same systems have been used to study thermoelectric performance of modulation doped samples.[14–16] Only a few silicides of transition metals have been reported to be semiconducting. These include Si-rich phases with transition metals from VI, VII, and VIII groups of the Periodic Table. Up to now, nine stable semiconducting transition metal silicide phases ($CrSi_2$, $MnSi_{1.73}$, β-$FeSi_2$, Ru_2Si_3, $ReSi_{1.75}$, OsSi, Os_2Si_3, $OsSi_2$, and Ir_3Si_5) with energy gaps in the range from 0.12 to 2.3 eV are known.[17–20] Here, we investigate the formation and thermoelectric properties of a nanostructured $Si_{0.8}Ge_{0.2}$ matrix with the embedded $FeSi_2$ phase. In the medium temperature range, the pure β-$FeSi_2$ is a p-type semiconductor with an orthorhombic crystal structure and transforms to tetragonal α-$FeSi_2$ phase, which has metallic properties at temperatures above 900°C. Since β-$FeSi_2$ possesses a higher thermoelectric power factor as compared to the doped silicon germanium, a composite material made of $Si_{0.8}Ge_{0.2}$ and β-$FeSi_2$ can be considered as a proper candidate for enhancing the thermoelectric properties. In order to synthesize n-type β-$FeSi_2$, we applied the approach reported in Ref. 21. Specifically, β-$FeSi_2$ was doped by Co via a mechanical alloying technique.

EXPERIMENTAL

Powders of SiGe doped by 2 at.% of P, β-$FeSi_2$, and Co of at least 99.99% purity were used for preparation of the samples. At the first step, $FeSi_2$ and Co powders were mixed in a desired proportion and mechanically alloyed in the planetary mill Fritch 7 Pulverisette. Subsequently, β-$Fe_{0.98}Co_{0.02}Si_2$ powder was mixed with $Si_{0,8}Ge_{0,2}$ powder and ball milled. The vial of the ball-mill and the milling media were made of zirconium oxide. The ball-to-powder weight ratio was 20:1, and the process was carried out in an argon atmosphere at a speed of 700 rpm. 1 wt. % of anti-friction and re-welding control agent (alcohol) was added to the vials. The samples were sintered from the prepared powder using two sintering techniques: spark plasma sintering (Labox 650, Sinter Land, Japan) and direct current sintering (universal simulator of metallurgical processes Gleeble 3800). The powders were put into a cylindrical graphite die, which was placed in a camera evacuated to a high vacuum. Uniaxial pressure was then applied through top and bottom plungers. Each plunger has a diameter of 12.7 mm and a length of 23 mm. The multiphase samples were prepared using the following sintering conditions (which were identical in both sintering methods): (1) the samples were pre-compressed at room temperature for 2 min, then the pressure was increased up to 60 MPa; (2) temperature of the samples was gradually raised to 1000–1100°C with a heating rate 10°C/s; and (3) after soaking time of 5 min, the pressure was reduced to 10 MPa and the samples were cooled to the room temperature for 15 min. During the consolidation cycle, the experimental parameters of temperature, applied pressure, current, voltage, and sample displacement were recorded continuously. Temperature was recorded by a thermocouple (Type R) inserted in a hole drilled into the die surface to a depth of 3.5 mm. The compacted disc samples have a dimension of 12.7 mm (diameter) × 2 mm (height). The samples were annealed at different temperatures for one week. The structure of the samples was examined by transmission electron microscopy (TEM). Samples for the TEM study were prepared by an ion polishing installation JEOL ION Slicer with the energy of the Ar ions at 4 keV. Studies of the phase composition of powdered samples were carried out on a Difrey-401 x-ray diffractometer at room temperature on Cr-K_α radiation (λ = 2,2909 Å). Density of the samples was determined by the Archimedes technique. Thermal conductivity measurements were carried out using a laser flash analysis system (Netzsch LFA 457) from room temperature up to 900°C. Specific heat was measured by a differential scanning calorimeter (DSC) Netzsch 204 F1. Electrical conductivity and the

Table I. Sintering parameters and volume density of the studied SiGe-$FeSi_2$ samples

Sample	Temperature, °C	Soaking time, min	Pressure, MPa	Density, % of theoretical
SPS 1000	1000	5	60	86.3
GL 1000	1000	5	60	83.4
SPS 1050	1050	5	60	89.7
GL 1050	1050	5	60	88.5
SPS 1100	1100	5	60	94.3
GL 1100	1100	5	60	92.8

Seebeck coefficient were measured simultaneously on bars measuring $1 \times 3 \times 12$ mm using a home-made transport measuring system (Cryotel Ltd.). The Hall resistivity was measured at room temperature in magnetic fields up to 10 kOe by a standard four-probe technique with current $I = 30$ mA passing through the sample.

RESULTS AND DISCUSSION

The nominal composition of the n-type material was P-doped $Si_{0.8}Ge_{0.2}$ with 10 at.% of β-$Fe_{0.98}Co_{0.02}Si_2$. After the milling process, the multiphase powder was subsequently sintered at absolutely equal conditions via the aforementioned techniques. The sintering parameters were chosen in such a way that allows one to compare our results with those reported in Ref. 7. The sintering conditions and the calculated density of all the samples are presented in Table I.

Samples sintered by the spark plasma sintering method are labeled as "SPS" while those sintered by the Gleable 3800 system are marked as "GL". Short soaking time and rapid heating was chosen to prevent recrystallization. Accumulated experimental data[22,23] showed that the SPS method does not lead to a significant grain growth and allows one to save nanocrystallite structure. At the same time, SPS technique allows one to obtain samples with a higher volume density at any sintering temperature (Table I). These facts make the SPS method more promising for achieving better results. Typical x-ray diffraction (XRD) patterns of powder and the sintered samples before and after annealing are presented in Fig. 1. The results of XRD analysis for the samples sintered and annealed under the other conditions were approximately identical.

Two apparent phases of SiGe solid solution and the α-$FeSi_2$ (tetragonal) are easily seen on the XRD patterns (Fig. 1). The FeSi phase was found in some samples sintered by Gleeble 3800, but this phase was not observed after homogenizing annealing. The fact that the orthorhombic β-$FeSi_2$ phase transforms to tetragonal α-$FeSi_2$ phase during high temperature sintering is clear and undeniable according to the XRD data. It should be noted that a long term annealing just below the phase transition temperature did not reverse completely the tetragonal α-$FeSi_2$ phase into the orthorhombic β-$FeSi_2$ phase. The XRD pattern of the powdered sample shows a significant broadening of the peaks due to an increase of the internal energy in the system caused by dispersing and increasing defect concentration in the sample. This effect partially remained in the sintered and annealed samples and

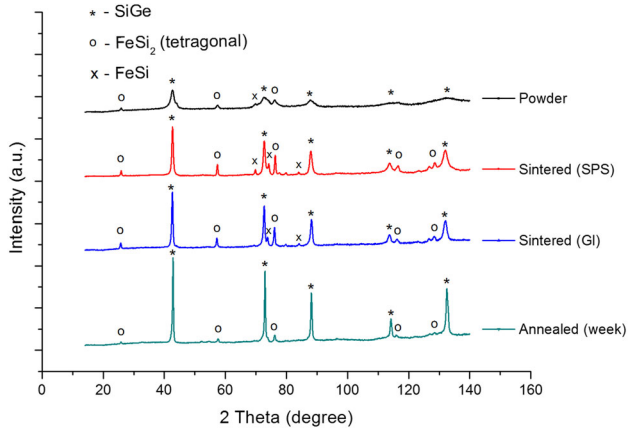

Fig. 1. XRD patterns collected for n-type SiGe-$FeSi_2$.

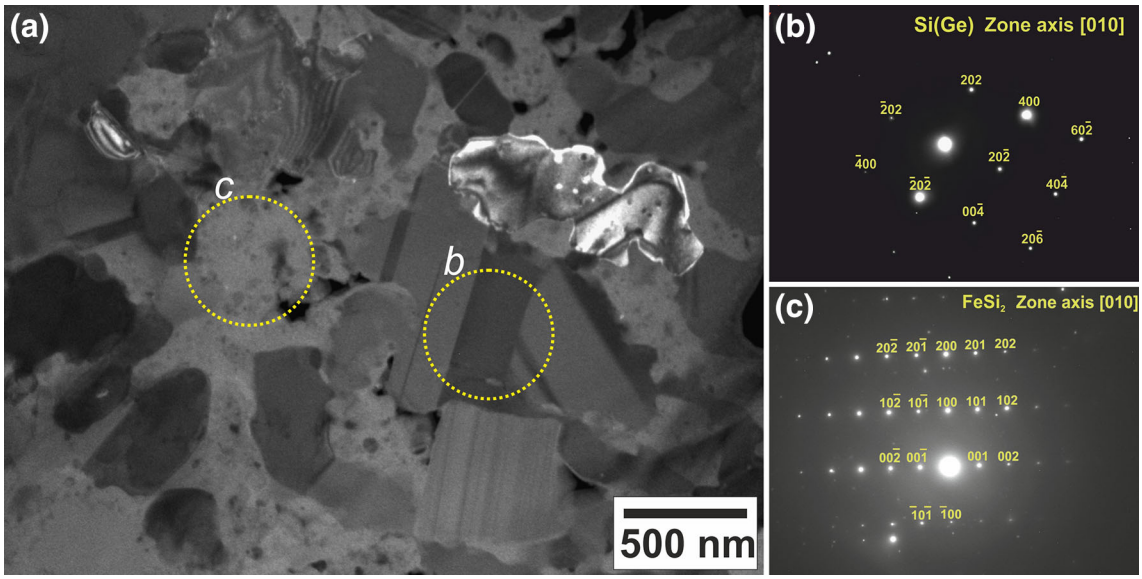

Fig. 2. (a) Dark-field TEM image of a typical microstructure of the SPS 1100 sample. Yellow regions on the micrograph mark the areas of SAED taken from a Si(Ge) single crystal along [010] zone axis (b) and an α-$FeSi_2$ single crystal along [010] zone axis (c).

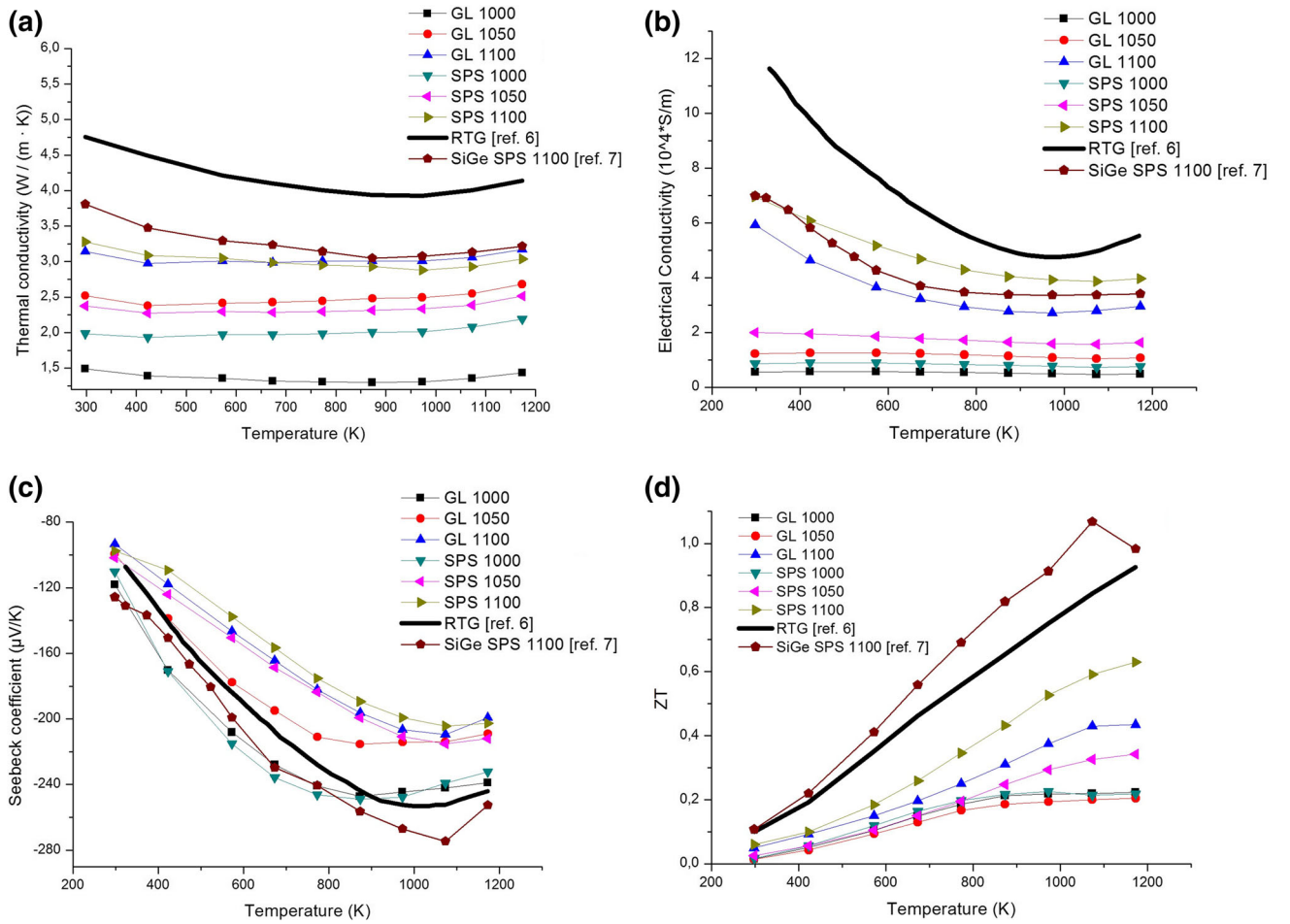

Fig. 3. Temperature dependence of thermoelectric properties of nanostructured multiphase SiGe-$FeSi_2$, the reference RTG sample (Ref. 6), and nanostructured SiGe sample sintered at 1100°C (Ref. 7): (a) thermal conductivity, (b) electrical conductivity, (c) Seebeck coefficient and (d) calculated *ZT*.

had a significant impact on thermal and transport properties.

A dark-field TEM image of the SPS 1100 sample is shown in Fig. 2a. The image was taken using a 111 type reflection on the ring diffraction pattern as an image forming reflection. The dark sharp-cornered particles were identified as SiGe on the basis of electron diffraction data (Fig. 2b). Moreover, the presence of typical silicon twin defects further indicated that these particles are a SiGe solid solution. $FeSi_2$ is mostly located at the boundaries of the SiGe particles. The diffraction pattern corresponding to $FeSi_2$ is shown in Fig. 2c. Obviously, the adhesion between the particles in a multiphase material slightly decreased in comparison with SiGe,[7] which causes formation of a significant amount of isolated pores.[24] Formation of the pores has a dramatic effect on the electrical transport properties of materials sintered at low temperatures. Temperature dependencies of thermal and electrical conductivities, the Seebeck coefficient and the calculated, from these data, *ZT* value are presented in Fig. 3. It can be seen from Fig. 3a that thermal conductivity k of all the multiphase samples is significantly lower as compared to that observed in the bulk radioisotope thermoelectric generator (RTG) sample (Ref. 6). For both consolidation techniques, thermal conductivity of the samples strongly depends on their sintering temperature (Fig. 3a). Evidently, the main reason for a large difference in thermal conductivity between the sintered samples is a considerable difference in the volume density of the samples, which strongly influences both lattice and electron components of the thermal conductivity. The lowest thermal conductivity value $k \sim 1.5$ W m^{-1} K^{-1} at room temperature was measured for the GL 1000 sample. However, this benefit was not large enough to overcome the loss in the electrical transport properties (Fig. 3b).

Electrical conductivity of the samples sintered at 1000°C and 1050°C demonstrates a significant drop, down to (1–2) $\times$ 10^4 S/m. Electrical conductivity curves measured for the SPS 1100 and GL 1100 samples show approximately the same behavior as that in the SiGe nanostructured sample and demonstrate a shape typical for highly-doped

Table II. Measured values of Hall coefficient R_H and calculated electron Hall mobility μ_e and carrier concentration n_e in the samples sintered at 1050°C and 1100°C

Sample	R_H, cm^3/C	μ_e, $cm^2/V\ s$	n_e, $cm^{-3}\times10^{19}$
SPS 1050	−1.14	223.5	0.55
GL 1050	−1.49	236.2	0.42
SPS 1100	−0.61	265.3	1.02
GL 1100	−0.65	270.9	0.98
SPS 1100 m [Ref. 7]	−0.54	257.1	1.16

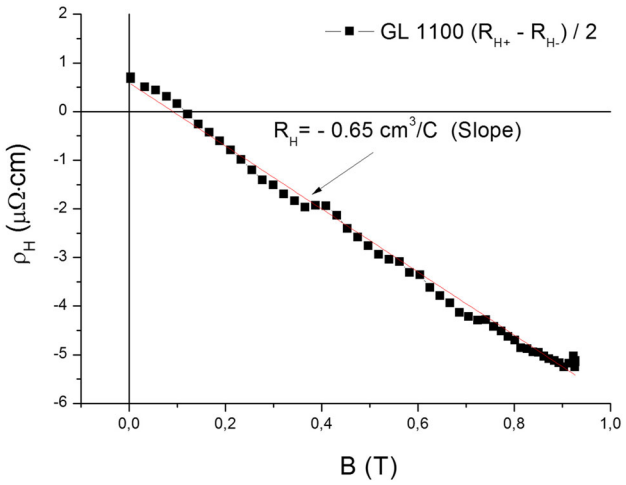

Fig. 4. Hall resistivity as a function of the magnetic field B in the GL 1100 sample. According to the obtained data, the drop of electrical conductivity can be mostly attributed to the drop of the carrier concentration. Meanwhile, the Hall mobility is also lower in the samples sintered at 1050°C.

semiconductors. As compared with the SPS 1100 and GL 1100 samples, other samples sintered at $T < 1100$°C have lower values of σ which did not alter significantly with increasing temperature. The Seebeck coefficient demonstrates a tendency toward decreasing its absolute values with the increase in the sintering temperature (Fig. 3c). This trend can be attributed to the influence of the α-$FeSi_2$ metallic phase, which injects a lot of charge carrier into the sintered nanostructured material leading to deviation from the optimum carrier concentration and decreasing Seebeck coefficient for the samples sintered at 1100°C. Meanwhile, the SPS 1000 and GL 1000 samples show significant growth of the Seebeck coefficient due to very low carrier concentration despite the contribution from α-$FeSi_2$ (see Table II). However, coupled with the electrical conductivity their power factor is lower as compared to the samples sintered at 1100°C. Calculated figure of merit of the studied SiGe-$FeSi_2$ samples is shown in Fig. 3d. As compared with the pure SiGe nanostructured sample sintered at the same conditions,[7] the SiGe-$FeSi_2$ samples have significantly lower ZT. The GL samples sintered at 1100°C and 1050°C show lower ZT values than the corresponding SPS samples. This is caused mainly by features of the SPS process that allow one simultaneously to preserve good electric transport properties and to decrease phonon transport. Measurements of the Hall coefficient R_H were carried out at room temperature for the samples sintered at 1100°C and 1050°C and also for the host SiGe sample. Typical behavior of the Hall resistivity is shown in Fig. 4. Positive Hall resistance seen at low magnetic fields is essentially related to a systematic error, which originates from an asymmetry in the voltage contacts. Within experimental error, the Hall resistivity is a linear function of the applied magnetic field. R_H was defined as a slope of the linear fit function. Results of calculations from the Hall coefficient values for carrier concentration and electron mobility in the measured samples are presented in Table II.

CONCLUSION

The multiphase nanostructured SiGe-$FeSi_2$ samples were synthesized both by SPS and direct current sintering techniques. The SPS technique turned out to be more suitable for consolidation of the SiGe-$FeSi_2$ samples. The highest $ZT \sim 0.6$ at 900°C was reached for nanostructured n-type SiGe doped by 10 at.% $FeSi_2$. The main reason for a rather low ZT value in the studied materials is the phase transition of semiconducting β-$FeSi_2$ to metallic α-$FeSi_2$. An optimal relation between the thermal and transport properties was obtained for the samples sintered at 1100°C.

ACKNOWLEDGEMENTS

The authors gratefully acknowledge the financial support of the Ministry of Education and Science of the Russian Federation in the framework of the Increased Competitiveness Program of NUST "MISiS" and financial support from RFBR (Grant #15-38-50811).

REFERENCES

1. D.M. Rowe, *Thermoelectrics Handbook: Macro to Nano* (CRC Press, Boca Raton, 2005).
2. H.J. Goldsmid, *Introduction to Thermoelectricity* (Springer Science & Business Media, Heidelberg, 2009).
3. Z. Chen, G. Han, L. Yang, L. Cheng, and J. Zou, *Prog. Nat. Sci.: Mater. Int.* 22, 535 (2012).

4. S. Novikov, A. Burkov, and J. Schumann, *J. Alloy. Compd.* 557, 239 (2013).
5. B. Kim, I. Kim, B. Min, M. Oh, S. Park, and H. Lee, *Electron. Mater. Lett.* 9, 4 (2013).
6. X. Wang, H. Lee, Y. Lan, G. Zhu, G. Joshi, D. Wang, J. Yang, A. Muto, M. Tang, and J. Klatsky, *Appl. Phys. Lett.* 93, 193121 (2008).
7. A. Usenko, D. Moskovskikh, M. Gorshenkov, A. Korotitskiy, S. Kaloshkin, A. Voronin, and V. Khovaylo, *Scr. Mater.* 96, 9 (2015).
8. L. Bulat, I. Drabkin, V. Karatayev, V. Osvenskii, Y.N. Parkhomenko, D. Pshenay-Severin, and A. Sorokin, *J. Electron. Mater.* 43, 2121 (2014).
9. N. Satyala, A. Rad, Z. Zamanipour, P. Norouzzadeh, J. Krasinski, L. Tayebi, and D. Vashaee, *J. Appl. Phys.* 115, 044304 (2014).
10. N. Mingo, D. Hauser, N. Kobayashi, M. Plissonnier, and A. Shakouri, *Nano Lett.* 9, 711 (2009).
11. P. Rouhani, Z. Zamanipour, J.S. Krasinski, D. Vashaee, and L. Tayebi, *Green Technologies Conference* (IEEE, Tulsa, OK, 2012), pp. 1–4.
12. Z. Zamanipour and D. Vashaee, *J. Appl. Phys.* 112, 093714 (2012).
13. K. Favier, G. Bernard-Granger, C. Navone, M. Soulier, M. Boidot, J. Leforestier, J. Simon, J. Tedenac, and D. Ravot, *Acta Mater.* 64, 429 (2014).
14. F. Dynys, A. Sayir, J. Mackey, and A. Sehirlioglu, *J. Alloy. Compd.* 604, 196 (2014).
15. H. Lange, *Phys. Status Solidi (b)* 201, 3 (1997).
16. M. Zebarjadi, G. Joshi, G. Zhu, B. Yu, A. Minnich, Y. Lan, X. Wang, M. Dresselhaus, Z. Ren, and G. Chen, *Nano Lett.* 11, 2225 (2011).
17. B. Yu, M. Zebarjadi, H. Wang, K. Lukas, H. Wang, D. Wang, C. Opeil, M. Dresselhaus, G. Chen, and Z. Ren, *Nano Lett.* 12, 2077 (2012).
18. S. Bux, R. Blair, P. Gogna, H. Lee, G. Chen, M. Dresselhaus, and J. Fleurial, *Adv. Funct. Mater.* 19, 2445 (2009).
19. I. Opahle, A. Parma, E.J. McEniry, R. Drautz, and G.K.H. Madsen, *New J. Phys.* 15, 105010 (2013).
20. K. Morikawa, H. Chikauchi, H. Mizoguchi, and S. Sugihara, *Mater. Trans.* 48, 2100 (2007).
21. S. Ur, *Thermoelectrics, 2003 Twenty-Second International Conference on - ICT* (IEEE, La Grande Motte, France, 2003), pp. 149–152.
22. N. Shkodich, A. Rogachev, S. Vadchenko, D. Moskovskikh, N. Sachkova, S. Rouvimov, and A. Mukasyan, *J. Alloy. Compd.* 617, 39 (2014).
23. D. Moskovskikh, Y. Lin, A. Rogachev, P. McGinn, and A. Mukasyan, *J. Eur. Ceram. Soc.* 35, 477 (2015).
24. P. Angelo and R. Subramanian, *Powder Metallurgy: Science, Technology and Applications* (PHI Learning Pvt. Ltd., New Delhi, 2008).